Available online at www.sciencedirect.com

ScienceDirect

Geochimica et Cosmochimica Acta 186 (2016) 32–48

Geochimica et Cosmochimica Acta

www.elsevier.com/locate/gca

Origin of the eclogitic clasts with graphite-bearing and graphite-free lithologies in the Northwest Africa 801 (CR2) chondrite: Possible origin from a Moon-sized planetary body inferred from chemistry, oxygen isotopes and REE abundances

H. Hiyagon [a,*], N. Sugiura [a], N.T. Kita [b], M. Kimura [c], Y. Morishita [d], Y. Takehana [a]

[a] Department of Earth and Planetary Science, Graduate School of Science, The University of Tokyo, Hongo 7-3-1, Tokyo 113-0033, Japan
[b] WiscSIMS, Department of Geoscience, University of Wisconsin-Madison, 1215 W, Dayton St., Madison, WI 53706, USA
[c] Faculty of Science, Ibaraki University, Bunkyo 2-1-1, Mito 310-8512, Japan
[d] Department of Geosciences, Shizuoka University, 836 Ohya, Suruga-ku, Shizuoka 422-8529, Japan

Received 4 February 2015; accepted in revised form 18 April 2016; Available online 27 April 2016

Abstract

In order to clarify the origin of the eclogitic clasts found in the NWA801 (CR2) chondrite (Kimura et al., 2013), especially, that of the high pressure and temperature (*P–T*) condition (~3 GPa and ~1000 °C), we conducted ion microprobe analyses of oxygen isotopes and rare earth element (REE) abundances in the clasts. Oxygen isotopic compositions of the graphite-bearing lithology (GBL) and graphite-free lithology (GFL) show a slope ~0.6 correlation slightly below the CR-CH-CB chondrites field in the O three-isotope-diagram, with a large variation for the former and almost homogeneous composition for the latter. The average REE abundances of the two lithologies show almost unfractionated patterns. Based on these newly obtained data, as well as mineralogical observations, bulk chemistry, and considerations about diffusion timescales for various elements, we discuss in detail the formation history of the clasts. Consistency of the geothermobarometers used by Kimura et al. (2013), suggesting equilibration of various elements among different mineral pairs, provides a strong constraint for the duration of the high *P–T* condition. We suggest that the high *P–T* condition lasted 10^2–10^3 years. This clearly precludes a shock high pressure (HP) model, and hence, strongly supports a static HP model. A static HP model requires a Moon-sized planetary body of ~1500 km in radius. Furthermore, it implies two successive violent collisions, first at the formation of the large planetary body, when the clasts were placed its deep interior, and second, at the disruption of the large planetary body, when the clasts were expelled out of the parent body and later on transported to the accretion region of the CR chondrites. We also discuss possible origin of O isotopic variations in GBL, and presence/absence of graphite in GBL/GFL, respectively, in relation to smelting possibly occurred during the igneous process(es) which formed the two lithologies. Finally we present a possible formation scenario of the eclogitic clasts.

Keywords: CR chondrite; Ion microprobe; Oxygen isotopes; REE abundances; High pressure minerals; Graphite-bearing clasts

* Corresponding author. Tel.: +81 3 5841 4592; fax: +81 3 5841 8321.
E-mail address: hiyagon@eps.s.u-tokyo.ac.jp (H. Hiyagon).

http://dx.doi.org/10.1016/j.gca.2016.04.030
0016-7037/

1. INTRODUCTION

Recent studies suggest that differentiated meteorite parent bodies formed *before* chondrite parent bodies based on ^{182}Hf–^{182}W chronology (Kleine et al., 2005, 2009; Qin et al., 2008) and calculations of thermal history of planetesimals assuming ^{26}Al as a heat source (Hevey and Sanders, 2006; Ghosh et al., 2006). The eclogitic clasts found in the Northwest Africa (NWA) 801 CR2 chondrite show igneous textures, such as lath-shaped graphite and euhedral olivine and orthopyroxene suggesting crystallization from melts (Kimura et al., 2013). Hence, presence of such clasts in a CR chondrite may also give further evidence that accretion of the differentiated planetesimals predates that of primitive chondrite parent bodies (Sokol et al., 2007; see also Abreu (2013) for similar arguments for the omphacite-bearing clast found in QUE 99177 CR3 chondrite).

The most significant feature of the clasts in the NWA 801 chondrite is the presence of a high pressure mineral assemblage (garnet and omphacite), similar to the terrestrial eclogite, suggesting their formation at 2.8–4.2 GPa and 940–1080 °C (Kimura et al., 2013). Such an eclogitic mineral assemblage has not been previously found in meteorites. Their mineralogical characteristics were reported in detail by Kimura et al. (2013), but their origin has not yet been clarified. Both static high pressure (HP) in a large planetary body and impact-induced HP seem possible based on the mineralogical study only.

Another distinct feature of the eclogitic clasts in NWA 801 is that they contain two distinct, graphite-bearing (GBL) and graphite-free (GFL), lithologies. The only achondrite group that contains graphite laths is ureilite. Therefore, GBL may have some affinity to ureilites and GFL possibly to primitive achondrites. Ureilites are considered to represent a mantle of a partially molten parent body, from which basaltic materials might have been mostly lost by explosive volcanism due to smelting which produced abundant CO gas (Warren and Kallemeyn, 1992; Scott et al., 1993). Smelting may have also played an important role for the formation of the two lithologies in the present clasts.

Graphite-free clasts with igneous textures are rare but sometimes found in chondrites (e.g., Sokol et al., 2007), but graphite-bearing clasts are much rarer and only a few were reported. Graphite-bearing xenoliths have been discovered in Krymka (Semenenko and Girich, 1995; Semenenko et al., 2005), which seem to be fragments of metamorphosed carbonaceous chondrite. Igneous graphite is present in enstatite chondrites (Rubin, 1997) and enstatite achondrites (Lowe et al., 2005). Recently, a graphite-bearing clast was found in QUE 99177 CR3 chondrite (Abreu and Brearley, 2007; Abreu, 2013). This clast also contains omphacite and these authors suggested the formation of this clast under high-pressure conditions. It contained relict chondrules and was considered to be a fragment of a metamorphosed carbonaceous chondrite. The present eclogitic clasts in NWA 801, on the other hand, do not contain such relict chondrules.

In order to better understand the origin of the eclogitic clasts found in the NWA 801 CR chondrite, we have conducted ion microprobe analyses of rare earth element (REE) abundances and oxygen isotopes on selected minerals. The REE data would provide information about the igneous processes on the parent body and O isotope data would provide information about the source materials of the clasts. In addition to these, diffusion calculations to explain possible chemical or isotopic variations in the clasts and to achieve equilibrium conditions for geothermobarometers would provide important constraints on the timescale(s) of the heating event(s). Based on these, we discuss the origin and formation history of the eclogitic clasts in the NWA 801 chondrite, which may have significant importance in understanding the early evolutionary history of the solar system.

2. TECHNICAL

Abundances of rare earth elements (REEs) were measured using an ion microprobe (Cameca-1270 at the National Institute of Advanced Industrial Science and Technology, Tsukuba, Japan). An O^- primary beam (1–2 nA, ~25 μm in diameter and 22.5 keV impact energy) was used for the analysis. Secondary ions were accelerated at 10 kV. Masses of 44 (^{44}Ca), and 138–178 (^{138}Ba, ^{139}La, ^{140}Ce, ^{141}Pr, ^{142}Nd, ^{147}Sm, ^{153}Eu, ^{158}Gd, ^{159}Tb, ^{163}Dy, ^{165}Ho, ^{166}Er, ^{169}Tm, ^{172}Yb, ^{175}Lu and ^{178}Hf) were analyzed with a single EM collector using a peak jumping mode. The analysis was performed at a low mass resolution (with fully open the exit slit) using an energy offset of −60 eV (with an energy slit width of 35 eV) to reduce interferences of complex ions at REE peaks (Zinner and Crozaz, 1986; Hiyagon et al., 2011). NIST 612 was used for the standard to obtain sensitivity factors for REEs relative to Ca (Table S1(a) in an electronic annex). Abundances of REEs were calculated assuming that the obtained signals were combinations of REE ions (REE^+) and REE-monoxide ions ($REEO^+$). Predetermined production ratios of $REEO^+/REE^+$ were used for the calculation. The calculation procedure was slightly modified from those of Fahey et al. (1987) and Hiyagon et al. (2011) due to smaller number of analyzed peaks. (Details of the present analytical parameters in comparison with those in Hiyagon et al. (2011) are described in Table S1(b) and Fig. S1(a) to (d) in an electronic annex.) The analyzed phases were chlorapatite, garnet, omphacite (Na–Al-rich pyroxene) and phlogopite; olivine and orthopyroxene (opx) were not measured because of their extremely low REE abundances suggested by our preliminary analyses. Some of the analysis spots contain multiple phases and the results for such spots must be treated carefully (see Section 4).

Oxygen isotopic compositions of olivine and opx were measured using an ion microprobe (Cameca ims-1280 at the University of Wisconsin-Madison, USA). The analytical conditions were basically the same as described in detail in Kita et al. (2009, 2010). We applied relatively higher primary Cs^+ beam intensities (~5 nA with 15 μm in diameter) in order to obtain higher secondary intensities of three oxygen isotopes ($^{16}O \sim 5 \times 10^9$, $^{17}O \sim 2 \times 10^6$, $^{18}O \sim 1 \times 10^7$ cps) and high precisions in $\delta^{18}O$ and $\delta^{17}O$ (<0.3‰ in 2SD). San Carlos olivine was analyzed as bracketing standard

and used for correction of instrumental bias during the unknown analyses.

3. BRIEF DESCRIPTION OF THE SAMPLE

3.1. Two lithologies: GBL and GFL

Petrography and mineralogy of the eclogitic clasts found in the NWA 801 were reported in detail in Kimura et al. (2013). Here we briefly summarize some of the characteristic features, which will be important in considering their formation processes.

Backscattered electron images of the three clasts (#2, #3 and #6), probably different portions of a single clast, are shown in Fig. 1(a)–(d). Two distinct lithologies, graphite-bearing lithology (GBL) and graphite-free lithology (GFL), can be recognized. Clast #2 consists of both GBL and GFL, while clasts #3 and #6 consist only of GFL and GBL, respectively. The two lithologies in clast #2 are well cemented together, suggesting that they assembled at high temperatures and/or they were annealed for a long time after the assembly.

3.2. Minerals

Enlarged views of GBL and GFL in clast #2 are shown in Fig. 2(a) and (b), respectively. Olivine, garnet, and omphacite are common minerals in both GBL and GFL, with minor amount of chlorapatite, Fe–Ni metal, troilite, and pentlandite. Orthopyroxene (opx) is present only in GBL, whereas phlogopite is present only in GFL. Olivine (typical grain size: ~20 μm in GBL and 20–40 μm in GFL) is chemically very homogeneous (Mg# from 66 to 68, where Mg# = Mg/[Mg + Fe] atomic ratio). Most of opx grains (~20 μm in size) are nearly homogeneous (Mg# 70–75), but a few coarse grains (50–80 μm in size) contain Mg-rich cores (Mg# 78–87), suggesting later Fe-enrichment by diffusion.

Garnet (5–30 μm in size) is nearly homogeneous, but omphacite (5–15 μm in size) is slightly variable in composition (Kimura et al., 2013). Chlorapatite (5–40 μm in size) is present both in GBL and GFL, but slightly enriched near the boundary of the two lithologies. Lath-shaped graphite (~5 μm wide and up to ~25 μm long) is present in GBL (~1 vol.%) along grain boundaries and within olivine and opx, suggesting formation from the melt.

Iron–Ni metal, troilite, pentlandite, and Fe oxides (probably weathering products of the former two) are more abundant in GFL than in GBL. Metal grains in GBL (typically ~10 μm in size) mostly occur as isolated grains and at grain boundaries of silicate minerals, while those in GFL (typically ~50 μm in size) mostly occur at grain boundaries, and in some places they are interconnected with each other to form channels or larger metal areas (up to ~200 μm in size; Fig. 1(a)).

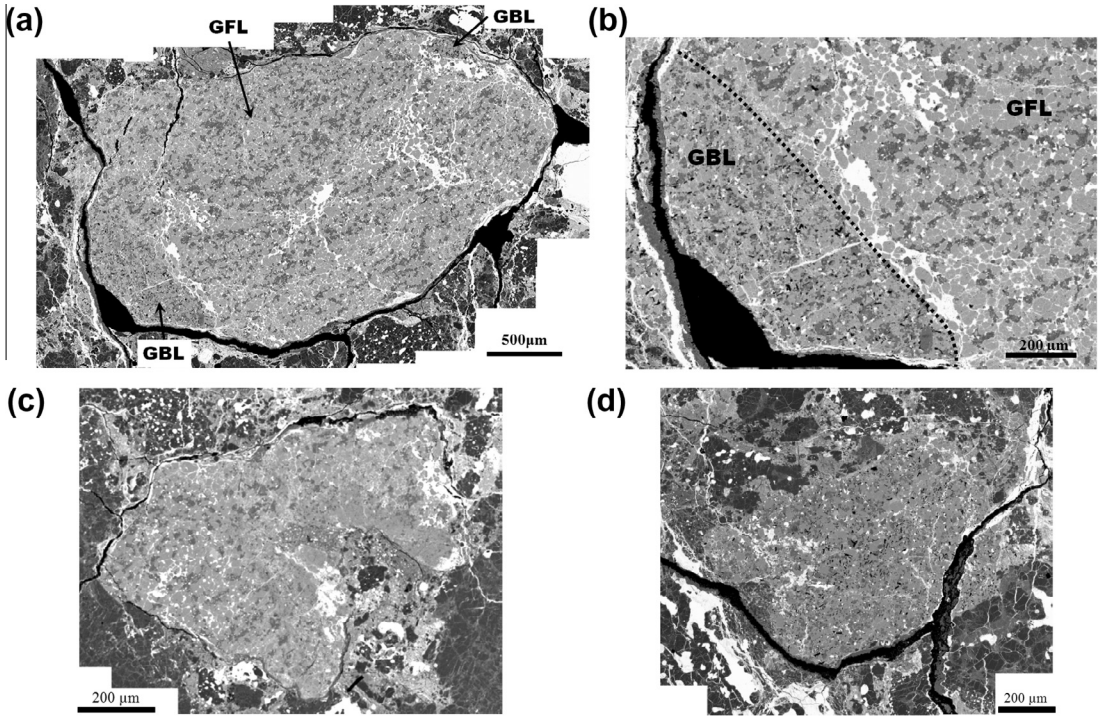

Fig. 1. (a) Back-scattered electron image of clast#2 (1.5 mm × 3 mm) in NWA 801 CR2 chondrite. It consists of two distinct lithologies: graphite-bearing lithology (GBL; occupying ~10 vol.% on the lower left and upper right corners of the clast) and graphite-free lithology (GFL; occupying ~90 vol.% in the central part of the clast). (b) Enlarged view of the lower-left corner of Fig. 1(a). Tiny, thin black grains in GBL are graphite (see Fig. 2(a) for details). GBL is slightly fine-grained than GFL. The boundary between GBL and GFL (dotted line) is well cemented. (c) Back-scattered electron image of clast#3 (1 mm × 0.8 mm). It consists only of GFL. (d) Back-scattered electron image of clast#6 (1 mm × 0.7 mm). It consists only of GBL.

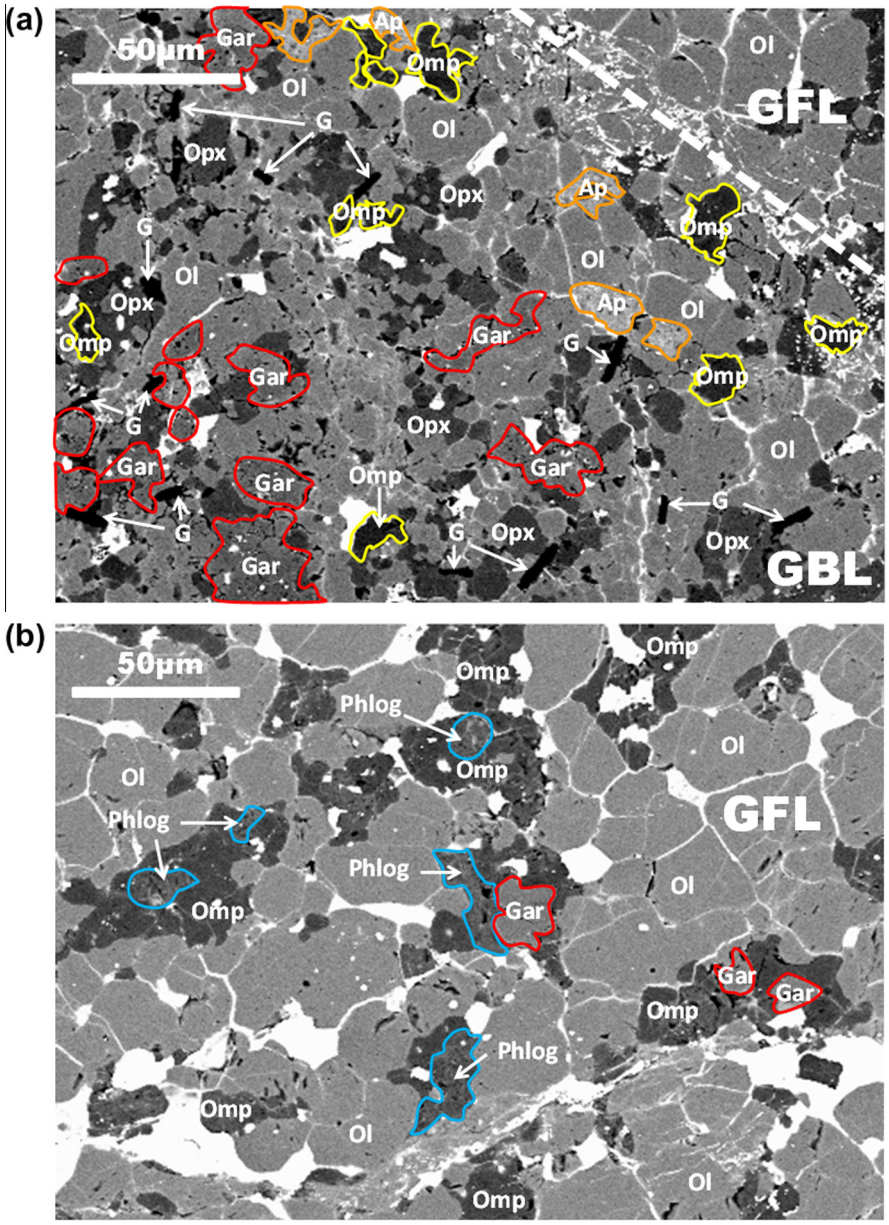

Fig. 2. (a) Back-scattered electron image of GBL (enlarged view). The boundary between GBL and GFL is shown as a broken line. Shown in the figure are olivine (Ol; light gray), Ca-poor pyroxene (Opx; gray), omphacite (Omp; dark gray rimmed by yellow lines), graphite (G; black elongated grains), garnet (Gar; rimmed by red lines) and chlorapatite (Ap; rimmed by orange lines). White grains are iron-nickel metal and sulfide. Veins shown here are mostly iron oxide, which is probably of terrestrial weathering product. (b) Back-scattered electron image of GFL (enlarged view). Olivine (Ol), omphacite (Omp), garnet (Gar; red lines) and phlogopite (Phlog; blue lines) are shown in the figure. White grains are mostly iron-nickel metal and sulfide. Veins are mostly iron oxide. Chlorapatite is not seen in this area. (For interpretation of the references to colour in this figure legend, the reader is referred to the web version of this article.)

3.3. Estimate of the *P–T* condition using geothermobarometers

A set of conventional geothermobarometers (7 formulas for 4 mineral pairs of opx-clinopyroxene (cpx, or omphacite), garnet-opx, garnet-cpx and garnet-olivine) were used by Kimura et al. (2013) to estimate the *P–T* condition for the formation of the clasts. All the obtained *P–T* relations, expressed as lines with various slopes on the *P–T* diagram, pass through a narrow *P–T* range of 2.8–4.2 GPa and 940–1080 °C (Fig. 6 of Kimura et al., 2013), suggesting formation of the clasts at this *P–T* condition. As will be discussed later, the consistency of geothermobarometers strongly suggests that equilibration was nearly attained for various elements among the mineral pairs at this high *P–T* condition. This will give a strong constraint for the origin of the high pressure and the formation process(es) of the clasts.

Table 1
Modal abundances of minerals in the two lithologies of clast #2 and clast #6.

Clast	Lithology	Olivine	Garnet	Opx	Omphacite	Phlogopite	Chlorapatite
Modal composition, 100% normalized (vol.%)*							
#2	GB	63.5	2.8	23.1	9.7	0.0	0.8
#6	GB	65.7	2.2	21.2	9.4	0.5	1.0
#2	GF	70.8	1.3	0.0	14.8	12.2	1.0
Modal composition, 100% normalized (wt.%)*							
#2	GB	65.8	3.1	21.4	9.0	0.0	0.7
#6	GB	67.1	2.4	20.2	9.0	0.4	0.9
#2	GF	73.2	1.4	0.0	14.3	10.2	0.9

* Excluding opaques (metal, sulfide, iron oxide), weathered regions, graphite and holes.

Table 2
Chemical compositions (CI-normalized abundances) of the two lithologies in the clasts, CR chondrites, and selected achondirtes.

	Si	Ti	Al	Cr	Fe	Mn	Mg	Ca	Na	K	P	Cl
Clast #2 (GFL)[1]	1.75	5.36	1.87	1.77	0.97	0.97	1.69	1.31	1.63	10.27	1.40	1.42
Clast #2 (GBL)[1]	1.88	0.69	0.95	1.36	0.97	1.05	1.76	1.12	0.99	<0.60	1.22	0.43
Clast #6 (GBL)[1]	1.85	0.69	0.87	1.31	0.96	1.05	1.76	1.18	0.99	<0.60	1.43	0.57
CR (Renazzo)[2]	1.49	2.55	1.29	1.44	1.31	0.93	1.45	1.37	0.82	0.61	1.00	–
CR (average)[3]	–	–	1.46	1.41	1.26	0.85	1.41	1.49	0.65	0.54	–	–
Acapulcoites (typical)[4]	–	2.29–3.90	0.93–1.88	0.88–1.99	0.90–1.41	1.32–1.46	1.38–1.56	1.08–1.69	0.97–1.45	0.57–1.15	–	–
Acapulcoites (primitive)[4]	–	1.84–3.44	1.14–1.18	1.11–1.22	1.70–1.93	1.03–1.20	1.06–1.47	0.95–1.48	0.92–1.10	0.74–1.31	–	–
Lodranites[4],[5]	1.68–2.09	0.83–4.59	0.27–0.90	0.62–1.45	0.54–1.29	1.11–2.11	1.82–2.75	0.75–1.46	0.06–0.58	<0.65	–	–
Ureilites[5]	1.77–1.81	0.83	0.10–0.43	1.21–1.84	0.55–0.81	1.34–1.56	2.12–2.42	0.74–1.00	0.03–0.29	0.03–0.63	0.25	–

[1] Calculated from modal compositions of the two lithologies in the clast (Table 1) and average compositions of the constituting minerals (Kimura et al., 2013). Opaque phases (Fe–Ni metal, sulfides, Fe-oxides, graphite) and holes are not included.
[2] Mason and Wiik (1962) (wet chemistry).
[3] Kallemeyn et al. (1994) (INAA).
[4] Patzer et al. (2004) (INAA).
[5] Mittlefehldt (2007) and references therein (compilation-INAA).

4. RESULTS

4.1. Bulk chemistry

Bulk chemical compositions of silicate part of the two lithologies are calculated from their modal abundances of minerals (Table 1) and average compositions of individual minerals (measured by EPMA; Kimura et al., 2013) assuming their appropriate densities. The results are listed in Table 2 and plotted in Fig. 3, along with the data for CR chondrites (Mason and Wiik, 1962; Kallemeyn et al., 1994) for comparison. Also listed in Table 2 are the data ranges for acapulcoites, lodranites and ureilites (Patzer et al., 2004; Mittlefehldt, 2007 and references therein). Note that the present data do not include opaque phases (Fe–Ni metal, etc.) because of high abundance of weathering products, and hence, the real Fe abundance (and to some extent those for other siderophile and chalcophile elements) must be higher than shown here. In spite of this limitation, we can still notice some important features of the two lithologies.

Incompatible elements (Ti, K, Na, Al and Cl) are enriched in GFL and depleted in GBL relative to the CI composition, suggesting that GFL contains higher

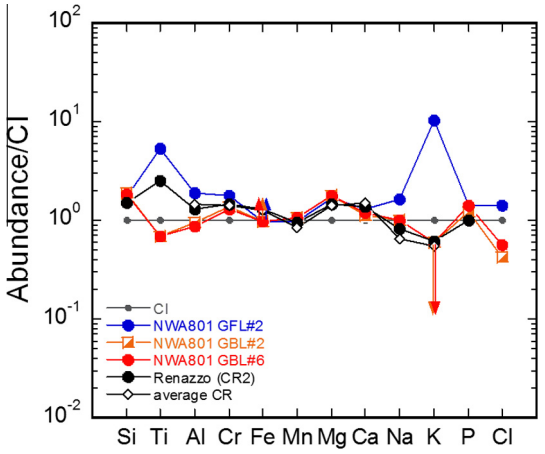

Fig. 3. CI-normalized elemental abundances of GBL (clast#2 and clast#6) and GFL (clast#2). Also shown for comparison is those of CR chondrites. The data for GBL and GFL do not include opaque minerals (Fe–Ni metal, sulfide, their weathering products and graphite) and holes, so that the real Fe content (and to some extent those of siderophile and chalcophile elements) must be higher than shown here. Only upper limits are shown for K data of GBL. Data sources: Mason and Wiik (1962) for Renazzo, Kallemeyn et al. (1994) for average CR, and Anders and Grevesse (1989) for CI.

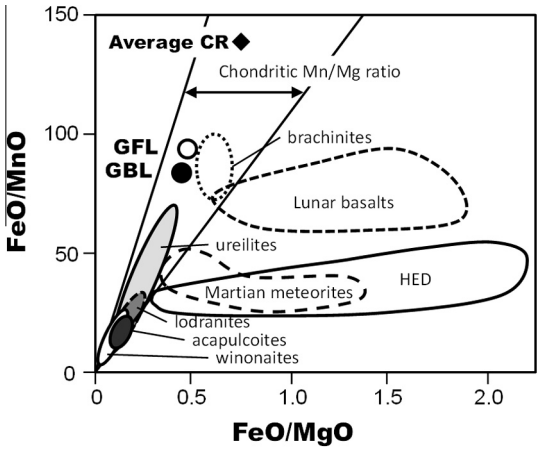

Fig. 4. An FeO/MnO vs FeO/MgO diagram for silicate portions of GFL and GBL. Also plotted are average CR chondrites (Kallemeyn et al., 1994), data fields of various achondrites, and the chondritic Mn/Mg range (3.9×10^{-3}–9.0×10^{-3}; shown by thin solid lines) (all the data plotted are bulk rock data; modified after Goodrich and Delaney, 2000). The Mn/Mg ratios for GBL (5.3×10^{-3}) and GFL (5.1×10^{-3}) of the NWA 801 clasts are well within the chondritic range, and are similar to those for average CR (5.4×10^{-3}), ureilites, and primitive achondrites (acapulcoites, lodranites, winonaites and brachinites). (Recent data for individual minerals of CR chondrite chondrules also show considerable variation but within the chondritic Mn/Mg range; Berlin et al., 2011; Schrader et al., 2015). Data of HED meteorites, lunar basalts and martian meteorites, originated from highly differentiated parent bodies, are plotted on far right of the chondritic region due to higher Fe/Mg ratios resulted from extensive igneous fractionations.

abundance of a melt (or a fluid) component but GBL is depleted in such a component. This is consistent with the igneous origin of the two lithologies suggested by mineralogical observations (Kimura et al., 2013).

In contrast, major elements (Si, Mg, Ca and possibly Fe) are almost unfractionated both in GBL and GFL, and their abundances are similar to those of CR chondrites (Fig. 3) and primitive or typical types of acapulcoites (Table 2; Patzer et al., 2004), but less fractionated than lodranites or ureilites (Table 2; see also Fig. S2(a) and (b) in an electronic annex).

Fig. 4 is a Fe/Mn vs Mg/Fe diagram (modified after Goodrich and Delaney, 2000). The Mn/Mg ratios of the two lithologies are well within the chondritic range and are similar to those for CR chondrites, primitive achondrites and ureilites. On the other hand, evolved achondrites (HED, Martian and Lunar meteorites) are plotted far right of the chondritic region, because of the higher Fe/Mg ratios resulted from igneous fractionations.

4.2. REEs

Rare earth element (REE) abundance patterns of various phases in GBL and GFL are provided in Table 4 and shown in Fig. 5(a) and (b), respectively. Note that some of the analysis spots contain multiple REE-bearing phases (see footnotes in Table 3), and hence, corrections may be

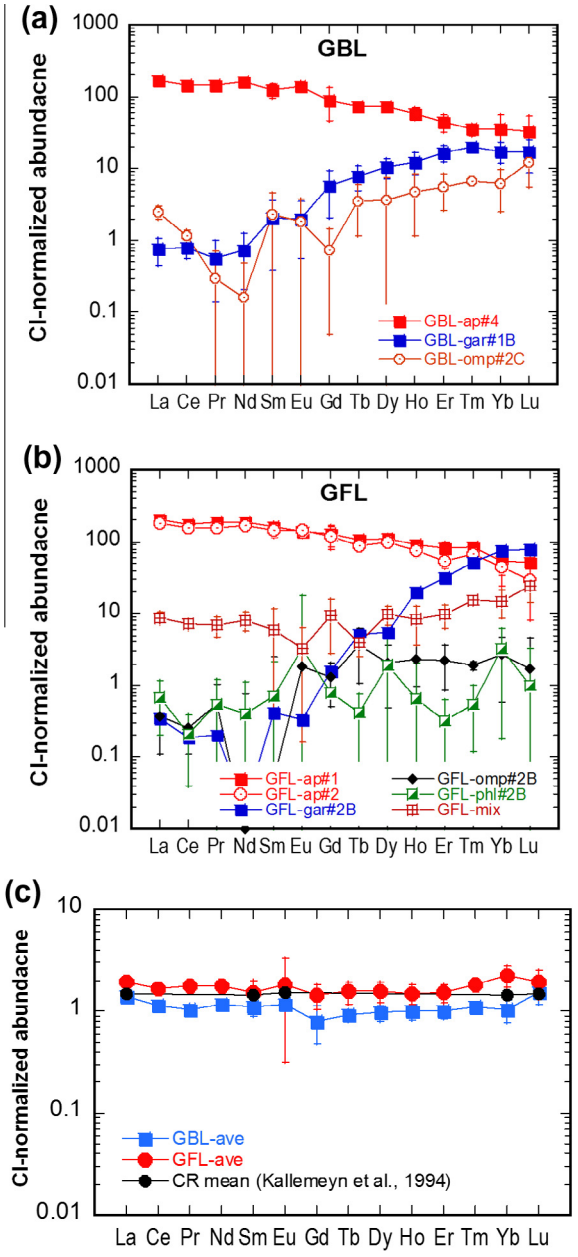

Fig. 5. (a) CI-normalized REE abundances in various minerals in GBL. Error bars are two-sigma. (b) Those in GFL. (c) Bulk REE abundances of GBL and GFL calculated from the present data (Table 4) and modal abundances of minerals (Table 1). Bulk GBL and GFL show almost flat REE patterns with the average abundances of ~1.2 × CI and ~1.8 × CI, respectively, which are not much different from that of CR chondrites (~1.5 × CI; Kallemeyn et al., 1994).

required. For example, REE data for omphacite in GFL (omphacite#2C) are corrected for a contribution from garnet.

Phosphate (chlorapatite) is the major carrier of LREEs in both GBL (~140 × CI) and GFL (~200 × CI), but HREE abundances decrease gradually from Gd toward Lu down to ~30 (GBL) or ~50 (GFL). In contrast, garnet is the major carrier of HREEs and the abundances increase

rapidly toward Lu up to ~20 × CI (GBL) or ~80 × CI (GFL). Both chlorapatite and garnet show slightly different REE abundance patterns between GBL and GFL, suggesting REEs are not in complete equilibrium between the two lithologies.

Bulk REE abundances of the two lithologies (calculated from Tables 1 and 3) are shown in Fig. 5(c) and Table 4, with those of CR chondrites (Kallemeyn et al., 1994) for comparison. Both GBL and GFL show nearly flat (unfractionated) REE patterns with the average abundances of ~1.2 × CI and ~1.8 × CI, respectively, which are not much different from those of average CR chondrites (~1.5 × CI). Note that REE abundances in eucrites (i.e., evolved achondrites) are much higher (typically >10 × CI; e.g., Warren and Kallemeyn, 1989; Barrat et al., 2000) and those in ureilites (considered to represent residual mantle) are much lower (much less than 1 × CI; e.g., Shimizu and Masuda, 1986; Kitts and Lodders, 1998). The unfractionated nature of REEs and P in the clasts makes a clear contrast with the other incompatible elements, which show strong enrichment in GFL or strong depletion in GBL. This suggests a possibility that P and REEs (mainly contained in chlorapatite) became redistributed at least partially between GBL and GFL in a later heating event.

4.3. Oxygen isotopes

Oxygen isotopic compositions of olivine and orthopyroxene (opx) in the clast #2 are given in Table 5 and shown in Fig. 6. All the data are distributed along a line with a slope of ~0.6 (0.63 ± 0.06 for all the data and 0.53 ± 0.15 for GBL data only; 2SE) located slightly below the fields of CR-CH-CB chondrites and the acapulcoite-lodranite clan. The GFL data are tightly clustered at the upper-right end of the distribution, whereas the GBL data are more scattered along the line. Note that the O isotopic variation in GBL (within a <400 μm area) is even larger than the whole variation of bulk acapulcoite-lodranite fields (Clayton and Mayeda, 1996; Greenwood et al., 2012). No clear correlation can be seen between the O isotopic composition and the distance from the GBL-GFL boundary (see Fig. S3 in an electronic annex).

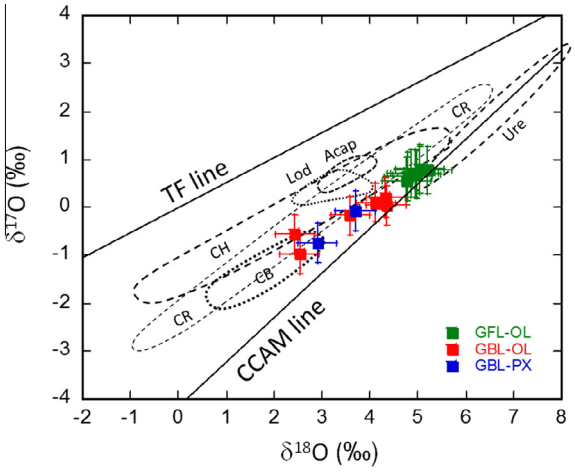

Fig. 6. Isotopic compositions of oxygen for olivine (OL) and Ca-poor pyroxene (PX) in GFL and GBL in clast#2. Terrestrial fractionation (TF) line and carbonaceous chondrite anhydrous minerals (CCAM) line are shown for references (Clayton et al., 1977). Also shown are the data fields of bulk CR chondrites, acapulcoites (Acap), lodranites (Lod) and ureilites (Ure) (Data sources: Clayton and Mayeda, 1996, 1999; Schrader et al., 2011, 2014).

5. DISCUSSION

5.1. Constraints from the bulk chemistry of the clasts

Enrichment of incompatible elements such as Ti, Al, Na, K and Cl (except for P and REEs) in GFL and their depletion in GBL (relative to the CI composition) suggest that the two lithologies have experienced gain or loss of a melt (or a fluid) phase, respectively, during their formation. However, major element abundances and Mn/Mg ratios (and bulk REE patterns as well) for both lithologies show almost no fractionation. This suggests that the igneous process(es) which produced GBL and GFL was (were) rather limited or localized one(s) and that planetary scale differentiation did not occur on their parent body.

The two lithologies, GBL and GFL, must have been juxtaposed *before* they experienced the high *P–T* condition (~3 GPa and ~1000 °C), because of their similarity in the presence of common high pressure minerals (garnet and omphacite) in spite of their difference in chemistry, mineralogy and oxygen isotopic composition. (The terms GBL and GFL here and in the next subsection are used for the two igneous lithologies *before* formation of garnet and omphacite at the high *P–T* condition.) It should be noted that the clear distinction between the two lithologies must be preserved during the high *P–T* event. This suggests that extensive melting did not occur during the formation of the high pressure minerals.

Phosphorus and REEs, whose major carrier is phosphate (chlorapatite), show almost no fractionation both in GBL and GFL (Figs. 3 and 5(c)). Because of their strong incompatibility, they must have been highly fractionated like other incompatible elements in the igneous process (es) which formed the two lithologies. The lack of large fractionation suggests that P and REEs were redistributed between GBL and GFL in a later heating event, either a high *P–T* event which formed the eclogitic clasts, or a later metamorphic event possibly occurred at a low pressure. As will be discussed in Section 5.4.3, a later metamorphic event is highly unlikely, so redistribution of P and REEs most likely occurred during the high *P–T* event.

5.2. Origin of GBL and GFL: possible role of smelting

The difference of the two lithologies, esp., presence or absence of graphite in GBL and GFL, respectively, must have been established *before* the high *P–T* event in which garnet and omphacite formed. Here we examine a possibility that smelting may have played an important role for the formation of the two lithologies.

Ferrous silicates are vulnerable to smelting in the presence of carbon at magmatic temperatures (e.g., Walker

Table 3
Concentrations of REEs and Ba in the Clast#2.

	GFL						GBL		
	Apatite#1	Apatite#2B[**]	Garnet#2B	Omphacite#2B	Phlogopite#2B	Mixed phase[***]	Apatite#4	Garnet#1B	Omphacite#2C[****]
Concentrations (ppm)									
Ba	86 ± 7	84 ± 7	8.0 ± 1.2	3.2 ± 0.5	420 ± 34	9.4 ± 1.2	68 ± 6	0.89 ± 0.22	3.3 ± 0.6
La	47 ± 2	43 ± 2	0.08 ± 0.08	0.09 ± 0.06	0.16 ± 0.11	2.0 ± 0.4	39 ± 2	0.18 ± 0.07	0.58 ± 0.12
Ce	110 ± 11	97 ± 10	0.12 ± 0.11	0.15 ± 0.09	0.13 ± 0.11	4.4 ± 0.7	90 ± 9	0.50 ± 0.14	0.72 ± 0.16
Pr	17 ± 2	15 ± 2	<0.06	0.05 ± 0.05	<0.11	0.65 ± 0.20	13 ± 2	0.05 ± 0.04	<0.07
Nd	87 ± 8	76 ± 7	<0.22	<0.35	<0.52	3.7 ± 1.1	75 ± 7	0.33 ± 0.24	<0.23
Sm	23 ± 5	21 ± 4	<0.25	<0.37	<0.31	0.88 ± 0.82	18 ± 4	0.30 ± 0.24	0.34 ± 0.34
Eu	7.6 ± 1.1	7.8 ± 1.2	<0.16	0.10 ± 0.10	<0.98[*]	0.18 ± 0.17	7.7 ± 1.3	0.11 ± 0.08	<0.20
Gd	25 ± 8	24 ± 8	0.31 ± 0.13	0.25 ± 0.15	0.16 ± 0.02	1.8 ± 1.3	18 ± 9	1.1 ± 0.7	0.15 ± 0.14
Tb	3.7 ± 0.3	3.1 ± 0.3	0.18 ± 0.18	0.13 ± 0.09	0.01 ± 0.01	0.14 ± 0.05	2.6 ± 0.3	0.28 ± 0.10	0.13 ± 0.08
Dy	27 ± 3	23 ± 3	1.3 ± 1.0	0.50 ± 0.38	0.45 ± 0.64	2.4 ± 0.7	17 ± 2	2.5 ± 0.8	0.87 ± 0.89
Ho	5.1 ± 0.7	4.2 ± 0.7	1.1 ± 0.8	0.13 ± 0.07	0.04 ± 0.08	0.46 ± 0.25	3.3 ± 0.6	0.69 ± 0.24	0.27 ± 0.20
Er	13 ± 2	8.8 ± 1.9	5.0 ± 2.6	0.36 ± 0.22	0.05 ± 0.05	1.6 ± 0.6	7.2 ± 2.0	2.7 ± 0.7	0.88 ± 0.47
Tm	2.0 ± 0.2	1.6 ± 0.2	1.2 ± 0.1	0.04 ± 0.01	<0.02	0.36 ± 0.04	0.8 ± 0.2	0.48 ± 0.05	0.16 ± 0.02
Yb	8.9 ± 3.4	7.3 ± 3.4	12 ± 3	0.43 ± 0.34	0.76 ± 0.56	2.4 ± 1.0	5.7 ± 3.3	2.8 ± 0.9	1.01 ± 0.60
Lu	1.2 ± 0.6	0.7 ± 0.5	1.9 ± 0.5	<0.11	<0.07	0.57 ± 0.24	0.8 ± 0.5	0.41 ± 0.20	0.29 ± 0.16
CI-normalized abundances[§]									
Ba	37 ± 3	36 ± 3	3.4 ± 0.5	1.4 ± 0.2	182 ± 15	4.1 ± 0.5	29 ± 3	0.4 ± 0.1	1.4 ± 0.3
La	203 ± 10	184 ± 10	0.3 ± 0.3	0.4 ± 0.3	0.7 ± 0.5	8.8 ± 1.5	168 ± 10	0.8 ± 0.3	2.5 ± 0.5
Ce	178 ± 18	157 ± 16	0.2 ± 0.2	0.2 ± 0.1	0.2 ± 0.2	7.2 ± 1.1	144 ± 15	0.8 ± 0.2	1.2 ± 0.3
Pr	185 ± 22	158 ± 20	<0.6	0.6 ± 0.5	<1.2	7.0 ± 2.2	145 ± 19	0.6 ± 0.4	<0.7
Nd	191 ± 17	167 ± 16	<0.5	<0.8	<1.1	8.1 ± 2.4	163 ± 16	0.7 ± 0.5	<0.5
Sm	160 ± 32	144 ± 30	<1.7	<2.5	<2.1	6.0 ± 5.6	125 ± 28	2.0 ± 1.6	2.3 ± 2.3
Eu	138 ± 21	144 ± 22	<2.7	1.8 ± 1.8	<18[*]	3.3 ± 3.1	142 ± 23	2.0 ± 1.4	<3.8
Gd	128 ± 42	120 ± ± 42	1.6 ± 0.7	1.3 ± 0.8	0.8 ± 0.1	9.3 ± 6.5	90 ± 43	5.7 ± 3.6	0.7 ± 0.7
Tb	105 ± 10	88 ± 9	5.0 ± 5.0	3.6 ± 2.6	0.4 ± 0.3	4.0 ± 1.4	72 ± 9	7.9 ± 2.9	3.5 ± 2.4
Dy	112 ± 14	98 ± 13	5.6 ± 4.3	2.1 ± 1.6	1.9 ± 2.7	9.9 ± 3.0	72 ± 10	11 ± 3	3.7 ± 3.7
Ho	91 ± ± 13	75 ± 12	20 ± 14	2.3 ± 1.3	0.7 ± 1.4	8.2 ± 4.5	59 ± 11	12 ± 4	4.8 ± 3.6
Er	82 ± 15	54 ± 12	31 ± 16	2.2 ± 1.4	0.3 ± 0.3	9.8 ± 3.7	44 ± 12	16 ± 4	5.5 ± 2.9
Tm	86 ± 9	67 ± 8	51 ± 5	1.9 ± 0.3	0.6 ± 0.4	15.3 ± 1.5	35 ± 7	20 ± 2	6.6 ± 0.7
Yb	55 ± 21	45 ± 21	75 ± 16	2.7 ± 2.1	3.2 ± 3.0	15.0 ± 6.4	35 ± 20	17 ± 6	6.2 ± 3.7
Lu	51 ± 23	29 ± 21	80 ± 21	<4.6	<3.2	24 ± 10	33 ± 21	17 ± 8	12 ± 7

[§] CI abundance by Anders and Grevesse (1989). Errors are 2σ.
[*] Large error due to high BaO contribution.
[**] Approximate composition: apatite (55%), omphacite (11%), olivine (34%).
[***] Approximate composition: garnet (55%), omphacite (32%), apatite (6%), olivine (7%).
[****] Approximate composition: olivine (50%), omphacite (40%), garnet (10%).

Table 4
Bulk compositions* of the two lithologies in the Clast #2.

	Concentrations in ppm		CI-normalized abundances	
	GFL	GBL	GFL	GBL
Ba	44.1 ± 3.5	0.79 ± 0.05	19.1 ± 1.5	0.34 ± 0.02
La	0.45 ± 0.03	0.33 ± 0.02	1.96 ± 0.11	1.41 ± 0.07
Ce	1.03 ± 0.10	0.70 ± 0.06	1.66 ± 0.16	1.12 ± 0.10
Pr	0.17 ± 0.02	0.10 ± 0.01	1.81 ± 0.22	1.05 ± 0.13
Nd	0.80 ± 0.09	0.53 ± 0.05	1.76±0.20	1.17±0.12
Sm	0.22 ± 0.07	0.16 ± 0.03	1.52 ± 0.48	1.11 ± 0.22
Eu	0.10 ± 0.08	0.06 ± 0.01	1.84 ± 1.53	1.18 ± 0.18
Gd	0.29 ± 0.08	0.16 ± 0.06	1.44 ± 0.39	0.80±0.32
Tb	0.06 ± 0.01	0.03 ± 0.00	1.57 ± 0.39	0.92 ± 0.13
Dy	0.38±0.09	0.23 ± 0.04	1.58 ± 0.38	0.97 ± 0.17
Ho	0.08 ± 0.02	0.06 ± 0.01	1.50 ± 0.33	1.00 ± 0.19
Er	0.25 ± 0.05	0.16 ± 0.03	1.53 ± 0.33	1.01 ± 0.18
Tm	0.043 ± 0.003	0.026 ± 0.002	1.81 ± 0.12	1.10 ± 0.08
Yb	0.37 ± 0.08	0.17 ± 0.04	2.25 ± 0.52	1.03 ± 0.25
Lu	0.05 ± 0.01	0.04 ± 0.01	1.93 ± 0.59	1.55 ± 0.37
Average of REEs			1.79 ± 0.12	1.16 ± 0.07

* Errors are two sigma.

Table 5
Oxygen isotopic compositions* of olivine and orthopyroxene in the clast #2.

Lithology	Pos#	Mineral	$\delta^{18}O$ (‰)	$\delta^{17}O$ (‰)	$\Delta^{17}O$ (‰)
GBL	#1	Orthopyroxene	3.70 ± 0.32	−0.07 ± 0.41	−1.99 ± 0.32
	#6	Olivine	4.33 ± 0.32	0.21 ± 0.41	−2.04 ± 0.32
	#5	Olivine	2.53 ± 0.32	−0.97 ± 0.41	−2.28 ± 0.32
	#2	Orthopyroxene	2.90 ± 0.32	−0.74 ± 0.41	−2.25 ± 0.32
	#3	Olivine	2.43 ± 0.32	−0.56 ± 0.41	−1.82 ± 0.32
	#7	Olivine	4.12 ± 0.32	0.10 ± 0.41	−2.04 ± 0.32
	#8	Olivine	3.59 ± 0.32	−0.17 ± 0.41	−2.03 ± 0.32
	#9	Olivine	4.34 ± 0.32	0.04 ± 0.41	−2.22 ± 0.32
GFL	#13	Olivine	4.79 ± 0.45	0.65 ± 0.50	−1.84 ± 0.27
	#14	Olivine	5.04 ± 0.45	0.78 ± 0.50	−1.84 ± 0.27
	#16	Olivine	4.86 ± 0.45	0.71 ± 0.50	−1.82 ± 0.27
	#17	Olivine	5.21 ± 0.45	0.78 ± 0.50	−1.93 ± 0.27
	#18	Olivine	4.98 ± 0.45	0.69 ± 0.50	−1.90 ± 0.27
	#19	Olivine	4.76 ± 0.45	0.55 ± 0.50	−1.93 ± 0.27
	#20	Olivine	4.94 ± 0.45	0.71 ± 0.50	−1.86 ± 0.27
	#21	Olivine	5.04 ± 0.45	0.81 ± 0.50	−1.81 ± 0.27

* Errors are 2 sigma.

and Grove, 1993). The smelting reaction may be written as: FeO (silicates) + C (graphite) → Fe (metal) + CO (gas). Since a gas phase appears only on the right-hand side, this reaction is highly pressure sensitive, that is, the reaction is suppressed at elevated pressures and promoted at lower pressures. The reaction is also dependent on FeO activity in silicates. The presence of graphite in GBL having an igneous texture, therefore, indicates that GBL formed at relatively high pressures (but not necessarily as high as ~3 GPa), where smelting was suppressed. The minimum pressure to prevent smelting can be calculated using the experimentally determined relation between Mg# of silicates (olivine or opx) and pressure as given by Walker and Grove (1993) (Fig. 7). If we take Mg# = 67 (average Mg# of olivine in both GBL and GFL), a minimum pressure of ~12 MPa is obtained. However, the presence of Mg-rich cores (with Mg# up to ~87) in large opx grains, which is consistent with igneous zoning, suggests that Mg# was ~87 or higher when GBL formed. Hence we obtain a minimum pressure of ~6.5 MPa (for Mg# = 87) or lower. The obtained pressures, <~6.5 MPa or ~12 MPa, correspond to the central pressures of planetesimals with <~60 km or ~90 km in radii, respectively, assuming mean density of 3000 kg/m^3 (Walker and Grove, 1993). Hence, we speculate that GBL formed at a deeper region of a relatively large planetesimal. Note that the fraction of graphite in GBL (~1 vol.%) is much lower than those in ureilites (up to 6.9–8 wt.%; Yamamoto et al., 1998; Smith et al., 2001). This may indicate that the initial C abundance of the source material for GBL was lower, or alternatively,

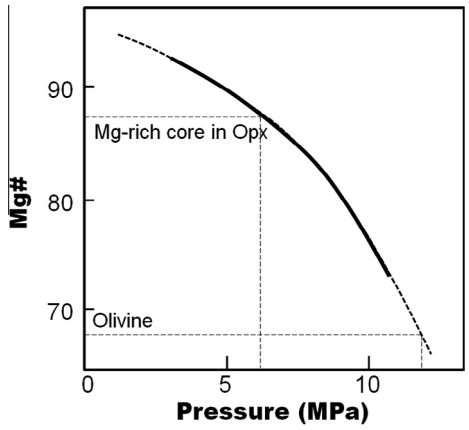

Fig. 7. Experimentally determined relation between Mg# of silicate crystals (olivine and opx) as a function of confining pressure at ~1200 °C for graphite + metal + gas-saturated assemblages (after Walker and Grove, 1993). For Mg# of 67 (average Mg# for olivine), we obtain ~12 MPa for the start of smelting (i.e., smelting occurs at a pressure of <12 MPa). For Mg# of 87 (highest Mg# in the cores of large opx grains), we obtain ~ 6.5 MPa for the start of smelting.

C was partially consumed during some degree of smelting occurred in GBL, or both.

The lack of graphite in GFL may be interpreted in two ways. (1) GFL formed at a shallow region of a planetesimal, where smelting easily occurred and graphite became completely consumed to form CO and lost. This, however, seems unlikely, because a melt-component-rich material like GFL must have been extensively lost from the parent body by explosive volcanism just like the case for ureilites (Warren and Kallemeyn, 1992; Scott et al., 1993). Hence, smelting may not be the cause for the lack of graphite in GFL. (2) Smelting never occurred in GFL due to absence of graphite in GFL. A possibility is transformation of originally contained carbon (organic or inorganic) into an oxidizing form like carbonate due to aqueous alteration *before* the igneous process that formed GFL, though carbonate formation is a rather slow process (Alexander et al., 2015). Another possibility is that the precursors of GFL and GBL were a chondrule-like material (containing no C) and a matrix-like material (containing C), respectively, just like a case of relict chondrules and matrix in the omphacitic clast of QUE 99177 (Abreu and Brearley, 2007; Abreu, 2013). This idea, however, seems inconsistent with the observation that phlogopite (implying former presence of H_2O) is only present in GFL but not in GBL.

At present, there is no evidence of smelting in the present clasts. The fact that we have GFL, a melt-component-rich material, in the clasts would indicate that explosive volcanism, if present, was not so extensive in the planetary body of GBL and GFL.

5.3. Shock HP model *vs* static HP model

In our petrographic and mineralogical study (Kimura et al., 2013), two possible origins are suggested for the high pressure (HP) condition of the clasts: a shock HP model and a static HP model. First, we briefly discuss characteristic features of the two models and their advantages and problems to explain the present observations.

5.3.1. Shock HP

Shock-induced HP is a good candidate, because numerous collisions between planetary bodies must have occurred during the solar system formation. However, a shock HP model have the following problems to explain the present observations.

(1) The estimated formation pressure of the clasts (~3 GPa) is unusually low compared with the typical HP reported for shock melt veins in meteorites (typically >20 GPa; e.g., Xie et al., 2001; Xie et al., 2006a,b; Ohtani et al., 2004; Baziotis et al., 2013). A possibility is that the estimated P–T condition of the clasts is a transient one attained during the P–T path after the shock. The idea of a transient P–T condition, however, seems contradictory to the consistency of the geothermobarometers, which in principle require a long enough time for equilibration of various elements among mineral pairs (see discussion below).

(2) A crucial problem of a shock HP model is the short duration of the high P–T condition. The duration of the shock τ is approximately given by the collision speed v and the impactor diameter d as $\tau = d/v$ (e.g., Gillet and El Goresy, 2013). If we assume a large impact event with $v = 5$ km/s (typical collision velocity for the asteroid belt; Bottke et al., 1994) and $d = 50$ km, τ is calculated to be 10 s. In fact, typical HP durations for the shock melt veins in meteorites are estimated to be milliseconds to at most a few seconds (e.g., Langenhorst and Poirier, 2000; Ohtani et al., 2004; Beck et al., 2005; Xie et al., 2006a). Hence, a typical τ may be ~10 s or less. This makes it difficult to form large high pressure minerals (e.g., ~30 μm-sized garnet) and to attain equilibrium conditions for various geothermobarometers.

(3) Homogenization of Fe/Mg ratios in olivine and most of opx (except for large opx grains) may not be possible during a short heating duration of the shock. Hence, another heating event, possibly a later metamorphic event at a low pressure, must be invoked in the shock HP model. Redistribution of P and REEs might also occur during this event. However, redistribution of various elements during a low pressure event would reset the geothermobarometric systems to indicate a low pressure.

5.3.2. Static HP

In a static HP model, it is assumed that the clasts were once placed deep interior of a large planetary body. In this case, it is easy to satisfy a long enough duration for the high P–T condition. As discussed by Kimura et al. (2013), it requires a Moon-sized planetary body of ~1500 km in radius to attain ~3 GPa near its center (Walker and Grove, 1993; Hartmann, 2005). Although such a large

asteroid is not observed in the current solar system, it is possible that it once existed but was later disrupted in the early solar system (see also Abreu, 2013), because it is a natural consequence that successively larger planetary bodies formed, or disrupted, through numerous (violent) collisions in the evolutionary processes from planetesimals to planets (e.g., Chambers, 2004; Bottke et al., 2006; Kokubo and Ida, 2012). A question for the static HP model is how the clasts were placed deep interior of a large planetary body and how they were excavated out of the planetary body.

5.4. Diffusion timescales for various elements

In our previous paper (Kimura et al., 2013), we preliminarily conducted diffusion calculations to explain the observed distribution of Fe/Mg ratio in olivine and opx. Here we present the results of our detailed calculations not only for Fe–Mg diffusion but also diffusion of O and other elements during various processes possibly occurred in the formation of the clasts. (See Table S4 in an electronic annex for summary of the present calculations.)

We assume a mineral grain to be approximated by a sphere with radius a, and we compare it with a typical diffusion length $L \sim (Dt)^{1/2}$ of a diffusing species, where D is the diffusion coefficient and t is the heating duration. We assume that equilibrium would be attained if $(Dt)^{1/2} > a$, but not attained if $(Dt)^{1/2} < a$.

5.4.1. Formation of garnet within a shock-melt

First, we consider a formation condition for large garnet grains (up to ~30 μm size) during a shock. Here we assume a case that the clasts became partially molten by shock heating and garnet formed in a silicate melt. The rate limiting process for garnet formation is probably diffusional transport of Al due to its lower diffusivity compared with other elements. Assuming that a shock-melt was kept at 1500 °C for $t \sim 10$ s and the diffusion coefficient of Al in a silicate melt D_{Al} to be $\sim 6 \times 10^{-11}$ m^2/s (Zhang et al., 2010; see Fig. 8), a diffusion length of Al is estimated to be ~24 μm, which is larger than the grain radius of garnet (a ~15 μm). (Note, however, that this estimation has uncertainties due to complex pressure dependence of D_{Al} in silicate melts; see e.g., Watson and Baxter, 2007.) Hence, formation of 30 μm-sized garnet may be possible even within a short duration of a shock. However, it is kinetically unlikely that only large garnet grains, instead of numerous micrometer-sized ones, were formed in the shock melt. In fact, the observed high pressure minerals in shock-melt veins in meteorites are generally of micrometers to submicrometers in size (e.g., Ohtani et al., 2004; Xie et al., 2006a).

In a static HP model, the heating duration would be long enough and large garnet grains may be safely formed. For example, some laboratory experiments show that ~10 μm-sized garnet grains were formed within 187 h at 1000 °C and the grain size became even larger (50–100 μm) at higher temperatures (Konzett et al., 2012).

5.4.2. Fe–Mg diffusion in olivine and orthopyroxene

Olivine is chemically very homogeneous (Mg# = 66–68) throughout the clasts, both in GBL (a ~10 μm) and GFL (a ~20 μm). Most of opx (typically a ~10 μm) is also nearly homogeneous (Mg# = 70–75), but some coarse grains (a ~25–40 μm) have Mg-rich cores (up to Mg# = 87). Heating conditions to explain these features can be estimated using diffusion calculations.

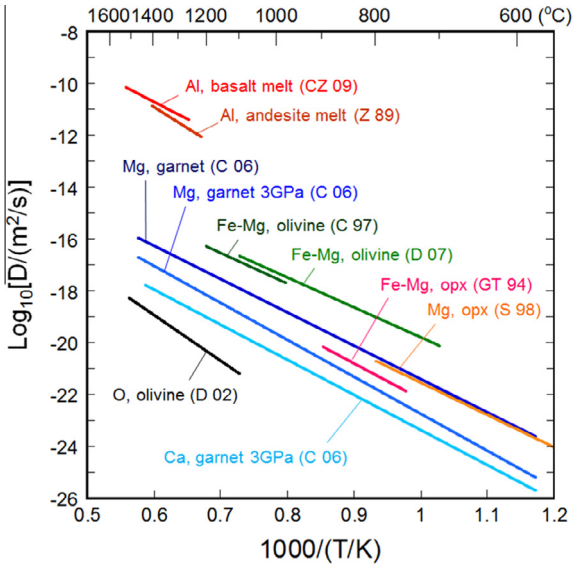

Fig. 8. Selected diffusion data (mostly at one atmospheric pressure) for various elements in minerals and melts used in the present discussion. Data sources: Al diffusion in basalt melt and andesite melt by Chen and Zhang (2009) (CZ 09) and Zhang et al. (1989) (Z 89), respectively, compiled by Zhang et al. (2010); Mg–Fe diffusion in olivine by Dohmen et al. (2007) (D 07); Mg self-diffusion in opx by Schwandt et al. (1998) (S 98); Mg–Fe diffusion in opx by Ganguly and Tazzoli (1994) (GT 94); Mg and Ca diffusion in garnet at 1 GPa by Carlson (2006) (C 06); oxygen diffusion in olivine by Dohmen et al. (2002) (D 02).

First, we consider a case for low pressures (~1 atm). For olivine, assuming the Fe–Mg diffusion coefficient $D_{Fe-Mg,olivine}$ at 1000 °C to be $\sim 1 \times 10^{-18}$ m^2/s (Chakraborty, 1997; Dohmen et al., 2007; see Fig. 8), a heating duration is calculated to be >10 years at 1000 °C. For opx, assuming $D_{Fe-Mg,opx}$ at 1000 °C to be $\sim 1 \times 10^{-19}$ m^2/s (Ganguly and Tazzoli, 1994; Schwandt et al., 1998; Fig. 8), a heating duration must be >30 years to homogenize completely Mg# in most of opx grains (a ~10 μm) but must be <200 years not to homogenize completely Mg# in large opx grains (a ~25–40 μm). Hence, the heating duration is estimated to be from 30 to 200 years. This heating duration automatically satisfies the heating duration to chemically homogenize olivine (>10 years).

Second, we consider a case for high pressures (~3 GPa). Diffusion coefficient at a high P–T condition ($D_{P,T}$) is related to that at 'zero pressure' and the same temperature (D_T) by the following equation: $D_{P,T} = D_T \times \exp(-PV_a/RT)$, where R is the gas constant and V_a is the activation volume (Béjina et al., 2003; Watson and Baxter, 2007). The Fe–Mg diffusion coefficient in olivine at ~3 GPa and 1000 °C is estimated to be $\sim 2 \times 10^{-19}$ m^2/s using $V_a = 5.3 \times 10^{-6}$ m^3 mol^{-1} (Holzapfel et al., 2007). This gives a heating duration of >60 years. Unfortunately, pressure

dependence is not known for Fe–Mg diffusion in opx, but if we assume a *P*-dependence similar to that for olivine, we may obtain $D_{Fe-Mg,opx}$ at ~3 GPa and 1000 °C to be $\sim 2 \times 10^{-20}$ m^2/s. This gives a heating duration for opx to be from ~140 years to ~900 years, or more roughly $\sim 10^2$–10^3 years (considering large uncertainties in the present estimation). Note that this calculation is too simple and another source of uncertainty comes from diffusion during heating to or cooling from the maximum temperature (~1000 °C), which would reduce the real heating time to some extent (depending on heating/cooling rates) (see e.g., McCoy et al., 1991).

5.4.3. Equilibrium condition for geothermobarometers

Conventional geothermobarometers are based on *P*- and *T*-dependent partitioning of various elements between different mineral pairs, such as, Ca–Mg exchange in the *M2* sites between the two pyroxenes, Fe^{2+}–Mg partition between garnet and common coexisting minerals (opx, clinopyroxene (cpx) and olivine), octahedral Al^{3+} content in opx coexisting with garnet, and so on (e.g., Krough Ravana and Paquin, 2003). The formulas to estimate the *P*–*T* conditions also include various corrections for minor element concentrations in minerals. Hence, equilibration of various elements (Fe, Mg, Ca, Al, Cr, Na, etc.) must be attained among these mineral pairs for the correct estimation of the *P*–*T* condition (see Table S5 in an electronic annex). In the case of the present clasts, all the geothermobarometers consistently indicate the formation condition within a narrow *P*–*T* range of 2.8–4.2 GPa and 940–1080 °C. This suggests that equilibration was nearly attained for various elements among these minerals at this high *P*–*T* condition. The important point is that not only the temperature (~1000 °C) but also the pressure (~3 GPa) must be maintained for a duration sufficient to equilibrate these elements among the mineral assemblage at this high *P*–*T* condition.

We have already estimated the diffusion timescales for Mg–Fe in olivine and opx to be 10^2–10^3 years at 1000 °C and ~3 GPa. This estimation is also applicable to the equilibrium condition for the geothermobarometers using olivine and opx as important mineral components. A question is whether or not the estimated high *P*–*T* duration (10^2–10^3 years) satisfies equilibrium conditions for other elements in different minerals.

The Ca–Mg interdiffusion coefficient at 1000 °C in clinopyroxene (cpx) is estimated to be $\sim 6 \times 10^{-22}$ m^2/s using the data for diopside obtained at ~2.5 GPa (nearly the same high *P* condition of the clasts; Brady and McCallister, 1983). Using this value and the typical grain radius (a ~7.5 μm), the diffusion timescale for Ca in omphacite (cpx) is calculated to be ~3000 years. Using diffusion coefficients of Mg, Fe, Mn and Ca in garnet at 1 GPa (e.g., $\sim 1 \times 10^{-19}$ m^2/s for Mg to $\sim 2 \times 10^{-20}$ m^2/s for Ca; Carlson, 2006) and their *P*-dependence (e.g., V_a $\sim 8.6 \times 10^{-6}$ m^3 mol^{-1} for Mg, $\sim 9.8 \times 10^{-6}$ m^3 mol^{-1} for Ca; Carlson, 2006), diffusion timescales in garnet (a ~15 μm) at 1000 °C and 3 GPa are calculated to be from ~400 years (for Mg) to ~2000 years (for Ca). The diffusion timescales for Ca in omphacite (~3000 years) and in garnet (~2000 years) are apparently longer than the high *P*–*T* duration estimated above (10^2–10^3 years). Note, however, that there are still considerable variations among the existing Ca diffusion data in cpx (Zhang et al., 2010, and references therein) and in garnet (Vielzeuf et al., 2007, and references therein). Note also that garnet and omphacite are new minerals formed during the high *P*–*T* event by decomposition of preexisting minerals (probably plagioclase and diopside) plus some reactions with olivine and opx. Furthermore, a small amount of a melt phase is also suggested during this high *P*–*T* event. In such a case, equilibration between the growing minerals (garnet and omphacite) and surrounding melt will be more easily attained than the above estimation. Hence, we may conclude that a duration of 10^2–10^3 years is a good estimation for the high *P*–*T* event.

An important inference from this calculation is that a later metamorphism (at a low pressure) is unlikely for the homogenization process of Fe/Mg ratios in olivine and most of opx. This is because heating at a low pressure would destroy consistency of the geothermobarometers. At a low pressure, the diffusion coefficients of Mg and Fe in garnet ($(2–3) \times 10^{-19}$ m^2/s; Carlson, 2006) are even higher than those in opx ($\sim 1 \times 10^{-19}$ m^2/s; Ganguly and Tazzoli, 1994; Schwandt et al., 1998). Therefore, if Fe–Mg homogenization occurred in olivine and opx at a low pressure, it must have occurred in garnet too. This means that the geothermobarometric systems using garnet-olivine, garnet-opx, and garnet-cpx pairs would be completely reset to indicate a low *P* condition, which however is not the case. Hence, we conclude that a late metamorphic event is highly unlikely.

In summary, the high *P*–*T* condition (~1000 °C and ~3 GPa) most likely lasted for 10^2–10^3 years in the formation of the present clasts. This clearly precludes a shock HP model, and hence, strongly supports a static HP model. During this high *P*–*T* event, the high pressure mineral assemblage (including garnet and omphacite) formed, olivine and most of opx became chemically homogenized (except for cores of large opx grains), and P and REEs were redistributed between GBL and GFL.

5.4.4. Diffusion timescale for oxygen and possible origin of its isotopic variation

The calculations below are based only on diffusion data at one atmospheric pressure, because *P*-dependence is not well known for O diffusion (e.g., Kushiro, 1983; Shimizu and Kushiro, 1984; Bryce et al., 1999; Reid et al., 2001). However, due to large difference in diffusion timescales of O and Fe–Mg (see below), the arguments may be valid even at ~3 GPa. Assuming $D_{O,olivine}$ at 1000 °C to be $\sim 6 \times 10^{-23}$ m^2/s (Dohmen et al., 2002; Fig. 8), the timescale for O diffusion in olivine (a ~10 μm) is calculated to be $\sim 5 \times 10^4$ years. This timescale is by far (about 2–4 orders of magnitude) longer than the timescales for Fe–Mg diffusion in olivine (>10 years) and in opx (30–200 years) at 1 atm. This suggests that the O isotopic variation originally present in GBL would not be affected by a later heating event that homogenized the Fe/Mg ratios in olivine and most of opx. Alternatively, if the O isotopic

variation in GBL was produced in a later heating event, the Fe/Mg ratios even in large opx grains would have become completely homogenized, which is inconsistent with the observations. Hence, we conclude that the O isotopic variation in GBL must have been established *before* the high *P–T* event, in which Fe/Mg ratios in olivine and most of opx became homogenized. The presence of phlogopite in GFL suggests that labile oxygen in the form of H_2O may have once existed in the clasts (in GFL). In such a "wet" condition, diffusivity of oxygen may be enhanced by a factor of ~10 for olivine (Costa and Chakraborty, 2008) and possibly also for pyroxene (for diopside; Farver, 1989; Ingrin et al., 2001). However, such an effect reduces the timescale for O diffusion only by a factor of ~10, i.e., still 1–3 orders of magnitude longer than that for Fe–Mg diffusion. Hence, the above conclusion would not be changed even in a "wet" condition.

Now we consider two possible models for the origin of the O isotopic variation in the clasts, esp., in GBL. The first possibility is that the O isotopic variation is the pristine one, which has not been completely erased by the igneous process(es) that formed GBL (and GFL). This may be possible if the degree of partial melting was very small and the heating duration was not long enough to homogenize O isotopic composition. The observed O isotopic variation may be related to similar variations seen in the data field of CR-CH-CB chondrites. Note, however, that the variation is extremely large considering the small area of the analysis (~400 μm area in GBL; see Fig. S3 in an electronic annex).

The second possibility is that the O isotopic variation was produced by the smelting reactions possibly occurred in the formation region of GBL. If smelting occurred partially and heterogeneously (possibly due to heterogeneous distribution of graphite), various degrees of O isotopic fractionation might be produced in silicates due to O isotope partitioning among CO gas, silicate minerals and a silicate melt. (Among them, O isotopic fractionation between the latter two may be very small; e.g., Eiler, 2001.), Removal of isotopically heavier CO (e.g., Onuma et al., 1972) would result in isotopically lighter O in silicates (Fig. 9). This is consistent with the observed slope for GBL data (0.53 ± 0.15; 2 SE), which is not different from the expected slope (~0.5). (If we include GFL data, however, the slope for all the data, 0.63 ± 0.06, becomes slightly larger than the expected one.) Various degrees of smelting would result in various degrees of silicate reduction, and hence, various Mg# in silicates, which, however, would have been completely erased in a later high *P–T* event (except for large opx grains). In this model, the initial O isotopic composition of the precursor of GBL must be located somewhere on or beyond the upper-right end of the GBL data field (see Fig. 9), possibly very close to the present GFL composition. In such a case, the precursor materials for GBL and GFL may have a common O isotopic composition located somewhere close to the present GFL composition, i.e., near the lower left end of the ureilites field. This may suggest some genetic relationships between the two.

A problem for the latter model, however, is that the smelting reaction (and possibly explosive volcanism) must be rather extensive in the parent body to produce such a large O isotopic variation. If this is the case, a melt-component-rich material like GFL must have been extensively lost from the parent body and may not be easily found (see arguments in Section 5.2). This makes the latter model less likely, though not impossible. If the former model is the case, the O isotopic variation is pristine, suggesting that the precursor material of the clasts is more closely related to CH-CB-CR chondrite groups than ureilites.

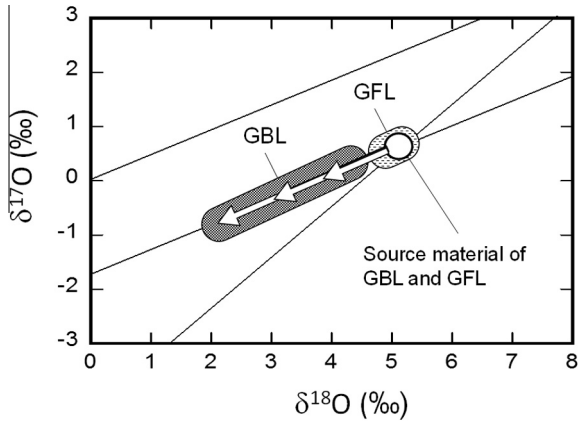

Fig. 9. A possible model for explaining the observed oxygen isotopic compositions of GBL and GFL (see text). It is assumed that smelting occurred partially and heterogeneously in GBL but never in GFL. Oxygen isotopes were partitioned between CO gas and silicates during smelting. Since the former had heavier O isotopic composition than the latter, loss of CO gas would result in various degrees of O isotopic fractionation in silicates. The precursor material for GBL must be located somewhere on the upper right end of the GBL data field, possibly close to the position of the present GFL. However, this model requires extensive smelting reactions (and possibly explosive volcanism) in the parent body of the clasts to produce such a large isotopic variation.

5.5. Comparison with the clast in QUE 99177 chondrite

There are some similarities and differences between the present clasts and the clast recently found in QUE 99177 (CR3) chondrite (Abreu and Brearley, 2007; Abreu, 2013). Both of them contain omphacite and lath-shaped graphite, as well as olivine and low Ca pyroxene, as common minerals. Graphite in the latter is much more abundant (~6.4 vol.%) and larger (up to ~70 μm long) than those in the present clasts (~1 vol.% and up to ~25 μm, respectively). Omphacite in the NWA 801 clasts is chemically more homogeneous, Na-rich, and Ca-poor compared with that in the QUE 99177 clast (mole fractions (%) of enstatite-ferrosilite, diopside-hedenbergite, jadeite and kosmochlor components are 19, 47, 34 and 10 on average for the former, and 11–40, 51–73, 2–31 and 0.2–3.8 for the latter). Garnet and metal are present in the former but absent in the latter. Phlogopite is only present in the former (in GFL), while amphibole is only present in the latter. It is also argued that the QUE clast was formed at high pressure conditions based on the unit cell volume of omphacite (Abreu, 2013). Unfortunately, there are no REE or O isotope data on the QUE clast available at present, so we can only make comparisons based on mineralogical and chemical data.

The QUE clast contains relict chondrules and a ~200 μm-sized olivine grain, suggesting its origin as a metamorphosed carbonaceous chondrite-like material (Abreu, 2013). In contrast, the NWA 801 clasts contain no relict chondrules and show more homogeneous texture within each lithology. It is interesting to note that the QUE clast also contains a graphite-bearing region (matrix) and graphite-free regions (relict chondrules), which is analogous to GBL and GFL in the NWA 801 clasts, respectively. However, this analogy may not be valid, because phlogopite (implying former presence of H_2O) is only present in GFL but not in GBL. Failure of this analogy and some of the differences given above (esp., absence of garnet in the QUE clast) seem to indicate different formation conditions for these two clasts.

5.6. Collisions between large planetary bodies

The estimated duration for the high P–T condition (~3 GPa and ~1000 °C) is in the order of 10^2–10^3 years. This timescale is much shorter than that for planetary growth (10^5–10^6 years; Chambers, 2004; Chambers et al., 2010; Kokubo and Ida, 2012), that for heating by ^{26}Al decay (mean life of ~10^6 years) or that for cooling of planetesimals (>10^6 years for >10 km-sized bodies; e.g., Hevey and Sanders, 2006). This may imply rather catastrophic event both at the beginning and at the end of the high P–T condition. We speculate the following scenario. First, a violent collision between ~1000 km-sized bodies occurred and formed a large planetary body of ~1500 km in radius, when the clasts were placed near its center and kept at ~3 GPa and ~1000 °C. Second, after 10^2–10^3 years, another violent collision occurred, which disrupted the planetary body, and the (eclogitic) clasts were expelled out of the planetary body and quenched. (Rapid cooling is also suggested by mineralogical considerations, e.g., survival of omphacite with a high-temperature structure; Kimura et al., 2013.) Later on, the clasts were transported to the accretion region of CR chondrites. Hence, two successive violent collisions might occur within a short time (10^2–10^3 years).

If this is the case, we have to consider the effect of shock HP produced by such violent collisions anyway. If a planetary body is non-porous, the effect of the collisional heating would be confined to extremely localized fractions of the planetary body, and globally averaged temperature increase would be only a few K (Keil et al., 1997), or at most 50 K even for a 1000 km body (Love and Ahrens, 1996). Note also that high pressure minerals in shocked meteorites are observed only within the shock-melt veins but not in the unmelted regions, suggesting that not only high P but also high T is necessary for the formation of high pressure minerals. This may explain at least partly the lack of the shock features in the clasts. Another possibility is that pre-existing fractures or voids might result in very heterogeneous energy deposition of the shock within the parent body (e.g., Asphaug et al., 1998), and hence, some fractions of the parent body material could survive without a large effect of the shock. Further studies are required to better understand the processes of such a large collisional event.

5.7. A possible scenario for the history of the eclogitic clasts

Below we present a possible scenario for the formation history of the eclogitic clasts in the NWA 801 chondrite.

1. The accretion time of the parent body (or bodies) for GBL and GFL may be sometime close to ~2 My after CAI formation, when enough (but not too much) heat source (^{26}Al) was present for partially melting the parent body (Hevey and Sanders, 2006; Ghosh et al., 2006). (Other heat sources, such as shock-heating, may also be possible, and in such a case, the formation time of the two lithologies cannot be well constrained.)
2. The two lithologies, GBL and GFL, formed through limited or localized melting in (a) parent body (bodies). GBL is depleted in a melt (or fluid) component, while GFL is enriched in it. A planetary-scale differentiation did not occur on their parent body (bodies). Considering similarities in GBL and GFL (e.g., both show almost unfractionated REE patterns, chondritic Mn/Mg ratios, and oxygen isotopic ratios plotted on the same correlation line), it seems more plausible that GBL and GFL formed in different regions (depths) of the same planetesimal.
3. The O isotopic variation in the clasts (in GBL) may be generated by O isotope partitioning between silicates and the CO gas during smelting possibly occurred heterogeneously in GBL. In this case, the source material might have an O isotopic composition similar to that of the present GFL. Alternatively, it may be inherited from the source materials with highly heterogeneous O isotopic compositions.
4. After the parent body (bodies) of GBL and GFL cooled and solidified, numerous collisions formed regolith layers on the surface of a planetesimal, and fragments of GBL and GFL were buried next to each other. The planetesimal grew larger and the two lithologies became loosely sintered.
5. A large collision between two large planetary bodies (~1000 km in size) resulted in formation of a large planetary body of ~1500 km in radius. At the same time, the clasts were placed near its center, where the high P–T condition (~3 GPa and ~1000 °C) was attained.
6. During heating near the center of the large parent body, decomposition of the preexisting minerals (including plagioclase and diopside) and formation of the high pressure mineral assemblage (garnet and omphacite) took place in the clasts. During this time, Fe/Mg ratios in olivine and most of opx (except for large grains) became homogenized, but heterogeneity in O isotopic composition in GBL was not erased. Also, redistribution of P and REEs partly occurred between the two lithologies.
7. After 10^2–10^3 years, another violent collision disrupted the large planetary body. Fragments of the eclogitic clasts were transported from deep interior out of the planetary body, which resulted in rapid cooling of the clasts. We speculate that these violent collisions probably occurred during an active stage of the planetary growth after dissipation of the solar nebula.

8. Finally, fragments of the eclogitic material, ejected from the disrupted large planetary body, were transported to the accretion region of the CR parent body (bodies). This happened at least later than ~3 Ma after CAI formation, which may be constrained by the ages of the CR chondrules (Nagashima et al., 2014; Schrader et al., 2013).

6. CONCLUSION

Based on newly obtained results of O isotopes and REE abundances, as well as the data of bulk chemistry, geothermobarometers and available diffusion coefficients, we discuss in detail the origin and formation history of the eclogitic clasts found in the NWA 801 (CR2) chondrite. The fact that the geothermobarometers consistently indicate a high P–T condition (~3 GPa and ~1000 °C) provides a strong constraint for the formation condition of the clasts, because it implies equilibration of various elements among different minerals at this high P–T condition. Based on diffusion calculations, the duration of the high P–T condition is estimated to be 10^2–10^3 years. This clearly precludes a shock HP model, and hence, strongly supports a static HP model. During this high P–T condition, the high pressure mineral assemblage (garnet and omphacite) formed, olivine and most of opx became chemically homogenized, and redistribution of REEs and P took place in the clasts. A static HP model requires a Moon-sized planetary body with a radius of ~1500 km to achieve a pressure of ~3 GPa near its center. In this model, two successive violent collisions are inferred; first, at the formation of the large planetary body, and second, at the disruption of the planetary body after 10^2–10^3 years. The present eclogitic clasts would provide a precious example for the igneous activities in planetesimals, frequent vigorous collisions and disruptions of large planetary bodies, and transportations and mixing of materials in different regions during an active stage of the planetary formation.

ACKNOWLEDGEMENTS

We thank Mr. H. Inaba for preparing the polished sections and Mr. K. Ichimura for keeping the SEM in a good condition. The manuscript has been greatly improved by the fruitful comments of two reviewers, Neyda Abreu and Devin Schrader, and the associate editor Munir Humayun. This study was supported by a Grant-in-aids of Ministry of Education, Science, Sport, and Culture of Japanese government, No. 23540567 to H. H. and No. 22540488 to M. K.

APPENDIX A. SUPPLEMENTARY DATA

Supplementary data associated with this article can be found, in the online version, at http://dx.doi.org/10.1016/j.gca.2016.04.030.

REFERENCES

Abreu N. M. and Brearley A. J. (2007) A unique graphite and amphibole-bearing clast in QUE 99177: an extensively metamorphosed xenolith in a pristine CR3 chondrite. *Lunar Planet. Sci. XXXVIII*, #2419.pdf.

Abreu N. M. (2013) A unique omphacite, amphibole, and graphite-bearing clast in Queen Alexandra Range (QUE) 99177: a metamorphosed xenolith in a pristine CR3 chondrite. *Geochim. Cosmochim. Acta* **105**, 56–72.

Alexander C. M. O'D., Bowden R., Fogel M. L. and Howard K. T. (2015) Carbonate abundances and isotopic compositions in chondrites. *Meteorit. Planet Sci.* **50**, 810–833.

Asphaug E., Ostro S. J., Hudson R. S., Scheeres D. J. and Benz W. (1998) Disruption of kilometer-sized asteroids by energetic collisions. *Nature* **393**, 437–440.

Anders E. and Grevesse N. (1989) Abundances of the elements: meteoritic and solar. *Geochim. Cosmochim. Acta* **51**, 197–214.

Barrat J. A., Blichert-Toft J., Gillet Ph. and Keller F. (2000) The differentiation of eucrites-The role of *in situ* crystallization. *Meteorit. Planet Sci.* **35**, 1087–1100.

Baziotis I. P., Liu Y., DeCarli P. S., Melosh H. J., McSween H. Y., Bodnar R. J. and Taylor L. A. (2013) The Tissint Martian meteorite as evidence for the largest impact excavation. *Nat. Commun.* **4**, 1404. http://dx.doi.org/10.1038/ncomms2414, www.nature.com /naturecommunications.

Beck P., Gillet Ph., El Goresy A. and Mostefaoui S. (2005) Timescales of shock processes in chondritic and martian meteorites. *Nature* **435**, 1071–1074.

Béjina F., Jaoul O. and Liebermann R. C. (2003) Diffusion in minerals at high pressure: a review. *Phys. Earth Planet. Inter.* **139**, 3–20.

Berlin J., Jones R. H. and Brearley A. J. (2011) Fe-Mn systematics of type IIA chondrules in unequilibrated CO, CR, and ordinary chondrites. *Meteorit. Planet. Sci.* **46**, 513–533.

Bottke W. F., Nolan, Jr., M. C., Greenberg R. and Kolvoord R. A. (1994) Velocity distributions among colliding asteroids. *Icarus* **107**, 255–268.

Bottke W. F., Nesvorny D., Grimm R. E., Morbidelli A. and O'Brien D. P. (2006) Iron meteorites as remnants of planetesimals formed in the terrestrial planet region. *Nature* **439**, 821–824.

Brady J. B. and McCallister R. H. (1983) Diffusion data for clinopyroxenes from homogenization and self-diffusion experiments. *Am. Mineral.* **68**, 95–105.

Bryce J. G., Spera F. J. and Stein D. J. (1999) Pressure dependence of self-diffusion in the $NaAlO_2$-SiO_2 system: compositional effects and mechanisms. *Am. Mineral.* **84**, 345–356.

Carlson W. (2006) Rates of Fe, Mg, Mn and Ca diffusion in garnet. *American Mineral.* **91**, 1–11.

Chakraborty S. (1997) Rates and mechanisms of Fe-Mg interdiffusion in olivine at 980° -1300°C. *J. Geophys. Res.* **102**, 1237–12331.

Chambers J. E. (2004) Planetary accretion in the inner solar system. *Earth Planet. Sci. Lett.* **223**, 241–252.

Chambers J. E., O'Brien D. P. and Davis A. M. (2010) Accretion of planetesimals and the formation of rocky planets. In *Protoplanetary Dust –Astrophysical and cosmochemical perspectives* (eds. D. Apai and D. S. Lauretta). Cambridge Univ. Press, New York, pp. 299–335.

Chen Y. and Zhang Y. (2009) Clinopyroxene dissolution in basaltic melt. *Geochim. Cosmochim. Acta* **73**, 5730–5747.

Clayton R. N. and Mayeda T. G. (1996) Oxygen isotope studies of achondrites. *Geochim. Cosmochim. Acta* **60**, 1999–2017.

Clayton R. N. and Mayeda T. K. (1999) Oxygen isotope studies of carbonaceous chondrites. *Geochim. Cosmochim. Acta* **63**, 2089–2104.

Clayton R. N., Onuma N., Grossman L. and Mayeda T. K. (1977) Distribution of the pre-solar component in Allende and other carbonaceous chondrites. *Earth Planet. Sci. Lett.* **34**, 209–224.

Costa F. and Chakraborty S. (2008) The effect of water on Si and O diffusion rates in olivine and implications for transport properties and processes in the upper mantle. *Phys. Earth Planet. Interiors* **166**, 11–29.

Dohmen R., Chakraborty S. and Becker H.-W. (2002) Si and O diffusion in olivine and implications for characterizing plastic flow in the mantle. *Geophys. Res. Lett.* **29**(21), 26-1–26-4. http://dx.doi.org/10.1029/2002GL015480, 2030***.

Dohmen R., Becker H.-W. and Chakraborty S. (2007) Fe-Mg diffusion in olivine I: experimental determination between 700 and 1,200 & #xB0;C as a function of composition, crystal orientation and oxygen fugacity. *Phys. Chem. Minerals* **34**, 389–407.

Eiler J. M. (2001) Oxygen isotopic variations of basaltic lavas and upper mantle rocks. *Rev. Mineral. Geochem.* **43**, 320–364.

Fahey A. J., Goswami J. N., McKeegan K. D. and Zinner E. (1987) ^{26}Al, ^{244}Pu, ^{50}Ti, REE and trace element abundances in hibonite grains from CM and CV meteorites. *Geochim. Cosmochim. Acta* **51**, 329–350.

Farver J. R. (1989) Oxygen self-diffusion in diopside with applications to cooling rate determinations. *Earth Planet. Sci. Lett.* **92**, 386–396.

Ganguly J. and Tazzoli V. (1994) Fe^{2+}-Mg interdiffusion in orthopyroxene: retrieval from the data on intracrystalline exchange reaction. *Am. Mineral.* **79**, 930–937.

Gillet P. and El Goresy A. (2013) Shock events in the Solar System: the message from minerals in terrestrial planets and asteroids. *Ann. Rev. Earth Planet. Sci.* **41**, 257–285.

Ghosh A., Weidenschilling S. J., McSween, Jr., H. Y. and Rubin A. (2006) Asteroidal heating and thermal stratification of the asteroid belt. In *Meteorites and the Early Solar System II* (eds. D. S. Lauretta and , Jr.H. Y. McSween). Univ. of Arizona, Tucson.

Goodrich C. A. and Delaney J. S. (2000) Fe/Mg-Fe/Mn relations of meteorites and primary heterogeneity of primitive achondrite parent bodies. *Geochim. Cosmochim. Acta* **64**, 149–160.

Greenwood R. C., Franchi I. A., Gibson J. M. and Benedix G. K. (2012) Oxygen isotope variation in primitive achondrites: the influence of primordial, asteroidal and terrestrial processes. *Geochim. Cosmochim. Acta* **94**, 146–163.

Hartmann W. K. (2005) *Moons and Planets*. Brooks/Cole, Belmount, p. 428.

Hevey P. J. and Sanders I. S. (2006) A model for planetesimal meltdown by ^{26}Al and implications for meteorite parent bodies. *Meteorit. Planet. Sci.* **41**, 95–106.

Hiyagon H., Yamakawa A., Ushikubo T., Lin Y. and Kimura M. (2011) Fractionation of rare earth elements in refractory inclusions from the Ningqiang meteorite: origin of positive anomalies in Ce. *Eu and Yb. Geochim. Cosmochim. Acta* **75**, 3358–3384.

Holzapfel C., Chakraborty S., Rubie D. C. and Frost D. J. (2007) Effect of pressure on Fe-Mg, Ni and Mn diffusion in $(Fe_xMg_{1-x})_2SiO_4$ olivine. *Phys. Earth Planet. Inter.* **162**, 186–198.

Ingrin J., Pacaud L. and Jaoul O. (2001) Anisotropy of oxygen diffusion in diopside. *Earth Planet. Sci. Lett.* **34**, 209–224.

Kallemeyn G. W., Rubin A. E. and Wasson J. T. (1994) The compositional classification of chondrites: VI. The CR carbonaceous chondrite group. *Geochim. Cosmochim. Acta* **58**, 2873–2888.

Keil K., Stöffler D., Love S. G. and Scott E. R. D. (1997) Constraints on the role of impact heating and melting in asteroids. *Meteorit. Planet. Sci.* **32**, 349–363.

Kimura M., Sugiura N., Mikouchi T., Hirajima T., Hiyagon H. and Takehana Y. (2013) Eclogitic clasts with omphacite and pyrope-rich garnet in the NWA 801 CR2 chondrite. *Am. Mineral.* **98**, 387–393.

Kita N. T., Ushikubo T., Fu B. and Valley J. W. (2009) High precision SIMS oxygen isotope analysis and the effect of sample topography. *Chem. Geol.* **264**, 43–57.

Kita N. T., Nagahara H., Tachibana S., Tomomura S., Spicuzza M. J., Fournelle J. H. and Valley J. W. (2010) High precision SIMS oxygen three isotope study of chondrules in LL3 chondrites: role of ambient gas during chondrule formation. *Geochim. Cosmochim. Acta* **74**, 6610–6635.

Kitts K. and Lodders K. (1998) Survey and evaluation of eucrite bulk compositions. *Meteorit. Planet. Sci.* **33**, A197–A213.

Kleine T., Mezger K., Palme H., Scherer E. and Münker C. (2005) Early core formation in asteroids and late accretion of chondrite parent bodies: evidence from ^{182}Hf-^{182}W in CAIs, metal-rich chondrites, and iron meteorites. *Geochim. Cosmochim. Acta* **69**, 5805–5818.

Kleine T., Touboul M., Bourdon B., Nimmo F., Mezger K., Palme H., Jacobsen S. B., Yin Q.-Z. and Halliday A. N. (2009) Hf-W chronology of the accretion and early evolution of asteroids and terrestrial planets. *Geochim. Cosmochim. Acta* **73**, 5150–5188.

Kokubo E. and Ida S. (2012) Dynamics and accretion of planetesimals. *Prog. Theor. Exp. Phys.* **01A308**, 23. http://dx.doi.org/10.1093/ptep/pts032.

Konzett J., Rhede D. and Frost D. J. (2012) The high PT stability of apatite and Cl partitioning between apatite and hydrous potassic phases in peridotite: an experimental study to 19 GPa with implications for the transport of P, Cl and K in the upper mantle. *Contrib. Mineral. Petrol.* **163**, 277–296.

Krogh Ravana E. and Paquin J. (2003) Thermobarometric methodologies applicable to eclogites and garnet ultrabasites. **5**. *EMU Notes Mineral.* **5**, 229–259, Chapter 8.

Kushiro I. (1983) Effect of pressure on the diffusivity of network-forming cations in melts of jadeitic compositions. *Geochim. Cosmochim. Acta* **47**, 1415–1422.

Langenhorst F. and Poirier J.-P. (2000) Anatomy of black veins in Zagami: clues to the formation of high-pressure phases. *Earth. Planet. Sci. Lett.* **184**, 37–55.

Love S. G. and Ahrens T. J. (1996) Catastrophic impacts on gravity dominated asteroids. *Icarus* **124**, 141–155.

Lowe J. J., Hill D. H., Dominik K. J., Lauretta D. S., Drake M. J. and Killgore M. (2005) NWA 2736: an unusual new graphite-bearing aubrite. *Lunar Planet. Sci. XXXVI*, #1913.pdf.

Mason B. and Wiik H. B. (1962) The Renazzo meteorite. *American Museum Novitates*, 2106****.

McCoy T. J., Scott E. R. D., Jones R. H., Keil K. and Taylor G. J. (1991) Composition of chondrule silicates in LL3-5 chondrites and implications for their nebular history and parent body metamorphism. *Geochim. Cosmochim. Acta* **55**, 601–619.

Mittlefehldt D. W. (2007) Achondrites. In *Meteorites, Comets and Planets: Treatise on Geochemistry Update 1* (ed. A. M. Davis). Elsevier, pp. 1–40. http://dx.doi.org/10.101/B0-08-043751-6/01064-1 (Chapter 1.11).

Nagashima K., Krot A. N. and Huss G. R. (2014) ^{26}Al in chondrules from CR2 chondrites. *Geochem. J.* **48**, 561–570. http://dx.doi.org/10.2343/geochemj.2.0346.

Ohtani E., Kimura Y., Kimura M., Takata T., Kondo T. and Kubo T. (2004) Formation of high-pressure minerals in shocked L6 chondrite Yamato 791384: constraints on shock conditions and parent body size. *Earth Planet. Sci. Lett.* **227**, 505–515.

Onuma N., Clayton R. N. and Mayeda T. K. (1972) Oxygen isotope cosmothermometer. *Geochim. Cosmochim. Acta* **36**, 169–188.

Patzer A., Hill D. H. and Boynton W. V. (2004) Evolution and classification of acapulcoites and lodranites from a chemical point of view. *Meteorit. Planet. Sci.* **39**, 61–85.

Qin L., Dauphas N., Wadhwa M., Masarik J. and Janney P. E. (2008) Rapid accretion and differentiation of iron meteorite parent bodies inferred from ^{182}Hf-^{182}W chronometry and thermal modeling. *Earth Planet. Sci. Lett.* **273**, 94–104.

Reid J. E., Poe B. T., Rubie D. C., Zotov N. and Wiedenbeck M. (2001) The self-diffusion of silicon and oxygen in diopside ($CaMgSi_2O_6$) liquid up to 15 GPa. *Chem. Geol.* **174**, 77–86.

Rubin A. E. (1997) Igneous graphite in enstatite chondrites. *Mineral. Mag.* **61**, 699–703.

Schrader D. L., Franchi I. A., Connolly, Jr., H. C., Greenwood R. C., Lauretta D. S. and Gibson J. M. (2011) The formation and alteration of the Renazzo-like carbonaceous chondrites I: implications of bulk-oxygen isotopic composition. *Geochim. Cosmochim. Acta* **75**, 308–325.

Schrader D. L., Nagashima K., Krot A. N., Ogliore R. C., Yin Q.-Z. and Amelin Y. (2013) Testing the distribution of ^{26}Al in the protoplanetary disk using CR chondrules. *Meteorit. Planet. Sci.* **76** (suppl.) #5141.

Schrader D. L., Davidson J., Greenwood R. C., Franchi I. A. and Gibson J. M. (2014) A water-ice rich minor body from the early solar system: the CR chondrite parent asteroid. *Earth Planet. Sci. Lett.* **407**, 48–60.

Schrader D. L., Connolly, Jr., H. C., Lauretta D. S., Zega T. J., Davidson J. and Domanik K. J. (2015) The formation and alteration of the Renazzo-like carbonaceous chondrites III: toward understanding the genesis of ferromagnesian chondrules. *Meteorit. Planet. Sci.* **50**, 15–50. http://dx.doi.org/10.1111/maps.12402.

Schwandt C. S., Cygan R. T. and Westrich H. R. (1998) Magnesium self-diffusion in orthoenstatite. *Contrib. Mineral. Petrol.* **130**, 390–396.

Scott E. R. D., Taylor G. J. and Keil K. (1993) Origin of ureilite meteorites and implications for planetary accretion. *Geophys. Res. Lett.* **20**, 415–418.

Semenenko V. P. and Girich A. L. (1995) Mineralogy of a unique graphite-containing fragment in the Krymka chondrite (LL3). *Mineral. Mag.* **59**, 443–454.

Semenenko V. P., Jessberger E. K., Chaussidon M., Weber I., Stephan N. and Wies C. (2005) Carbonaceous xenoliths in the Krymka LL3.1 chondrite: mysteries and established facts. *Geochim. Cosmochim. Acta* **69**, 2165–2182.

Shimizu N. and Kushiro I. (1984) Diffusivity of oxygen in jadeite and diopside melts at high pressures. *Geochim. Cosmochim. Acta* **48**, 1295–1303.

Shimizu H. and Masuda A. (1986) REE patterns of eucrites and their genetic implications. *Geochim. Cosmochim. Acta* **50**, 2453–2460.

Smith C. L., Franchi I. A., Wright I. P., Grady M. M. and Pillinger C. T. (2001) New data on carbon isotope compositions of some ureilites. *Lunar Planet. Sci. XXXII*, #1878.

Sokol A. K., Bischoff A., Marhas K. K., Mezger K. and Zinner E. (2007) Late accretion and lithification of chondritic parent bodies: Mg isotope studies on fragments from primitive chondrites and chondritic breccias. *Meteorit. Planet. Sci.* **42**, 1291–1308.

Vielzeuf D., Baronnet A., Perchuk A. L., Laporte D. and Baker M. B. (2007) Calcium diffusivity in alumino-silicate garnets: an experimental and ATEM study. *Contrib. Mineral. Petrol.* **154**, 153–170.

Walker D. and Grove T. (1993) Ureilite smelting. *Meteoritics* **28**, 629–636.

Warren P. H. and Kallemeyn G. W. (1989) Geochemistry of polymict ureilite EET83309, and a partially-disruptive impact model for ureilite origin. *Meteoritics* **24**, 233–246.

Warren P. H. and Kallemeyn G. W. (1992) Explosive volcanism and the graphite-oxygen fugacity buffer on the parent asteroid (s) of the ureilite meteorites. *Icarus* **100**, 110–126.

Watson E. B. and Baxter E. F. (2007) Diffusion in solid-Earth systems. *Earth Planet. Sci. Lett.* **253**, 307–327.

Xie X., Chen M. and Wang D. (2001) Shock-related mineralogical features and P-T history of the Suizhou L6 chondrite. *Eur. J. Mineral.* **13**, 1177–1190.

Xie Z., Sharp T. G. and DeCarli P. S. (2006a) High-pressure phases in a shock-induced melt vein of the Tenham L6 chondrite: constraints on shock pressure and duration. *Geochim. Cosmochim. Acta* **70**, 504–515.

Xie Z., Sharp T. G. and DeCarli P. S. (2006b) Estimating shock pressures based on high-pressure minerals in shock-induced melt veins of L chondrites. *Meteorit. Planet. Sci.* **41**, 1883–1898.

Yamamoto T., Hashizume K., Matsuda J.-I. and Kase T. (1998) Multiple nitrogen isotopic components coexisting in ureilites. *Meteorit. Planet. Sci.* **33**, 857–870.

Zhang Y., Walker D. and Lesher C. E. (1989) Diffusive crystal dissolution. *Contrib. Mineral. Petrol.* **102**, 492–513.

Zhang Y., Ni H. and Chen Y. (2010) Diffusion data in silicate melts. *Rev. Mineral. Geochem.* **72**, 311–408.

Zinner E. and Crozaz G. (1986) A method for the quantitative measurement of rare earth elements in the ion microprobe. *Int. J. Mass Spectrom. Ion Process* **69**, 17–38.

Associate editor: Munir Humayun